Guo *et al. Satellite Navigation* (2023) 4:9
https://doi.org/10.1186/s43020-023-00098-2

Satellite Navigation
https://satellite-navigation.springeropen.com/

ORIGINAL ARTICLE

Open Access

Instantaneous velocity determination and positioning using Doppler shift from a LEO constellation

Fei Guo[1,2*], Yan Yang[1], Fujian Ma[3], Yifan Zhu[1], Hang Liu[1] and Xiaohong Zhang[1,2]

Abstract

To provide backup and supplementation for the Global Navigation Satellite System (GNSS), Doppler shift from Low Earth Orbit (LEO) satellites can be used as signals of opportunity to provide positioning, navigation, and timing service. In this contribution, we first investigate the model and performance of instantaneous velocity determination and positioning with LEO satellites. Given a LEO constellation with 288 satellites, we simulate Doppler shift observations at nine multi-GNSS experiment stations. Owing to the lower orbit, the performance of LEO velocity determination is much more sensitive to the initial receiver position error than that of GNSS. Statistical results show that with the initial receiver position error increased from 0.1 to 10 m, the Root Mean Square Errors (RMSEs) increase from 0.73 to 2.65 cm/s, 0.68 to 2.96 cm/s, and 1.67 to 4.15 cm/s in the east, north, and up directions, respectively. The performances with GPS are compared with GPS + LEO, and it is found that LEO Doppler shift observations contribute to GPS velocity determination. As for LEO Doppler positioning, even if more than 30 visible LEO satellites are available, the position dilution of precision values can reach several hundreds. Assuming that the error of LEO Doppler measurements is 0.01 m/s, the instantaneous Doppler positioning accuracy can achieve about a few meters, which is comparable to that of GNSS pseudorange positioning. A constant velocity model is adopted for state transition. Static LEO Doppler positioning results show that an accuracy at centimeter to decimeter level can be achieved after solution convergence. For a static simulated kinematic positioning test, the RMSEs range from a few decimeters to several meters in different regions by giving different constraints. For a dynamic positioning test, the RMSEs are about 2–3 m in high latitude region.

Keywords Low earth orbit (LEO), GNSS, Doppler shift, Velocity determination, Instantaneous Doppler positioning

Introduction

GNSS is the main approach to offering PNT service and has about 130 available satellites at present (Lu et al., 2020). However, it is difficult to guarantee the continuity, anti-interference and anti-spoofing performance of the GNSS signals due to serious attenuation in the spreading process (Borio et al., 2016; Ioannides et al., 2016; Wang et al., 2020). In recent years, LEO satellites are employed to provide backup and supplementation for GNSS PNT services (Enge et al., 2012). Some LEO-based PNT approaches require satellites with navigation payloads as LEO-enhanced GNSS (LeGNSS) (Ge et al., 2018), while others use Doppler shift measurements to develop LEO PNT in opportunistic navigation (OpNav) (Kassas et al., 2021). The former has proved that LEO satellites contribute to faster convergence and ambiguity fixing in Precise Point Positioning (PPP) (Li et al., 2019a) and Real-Time Kinematic (RTK) (Li et al., 2019b). However,

*Correspondence:
Fei Guo
fguo@whu.edu.cn
[1] School of Geodesy and Geomatics, Wuhan University, Wuhan 430079, China
[2] Hubei Luojia Laboratory, Wuhan 430079, China
[3] Institute of Telecommunication and Navigation Satellites, China Academy of Space Technology, Beijing, China

the medium-long stability of an onboard LEO satellite clock affects not only its timekeeping ability but also the ranging accuracy of LeGNSS positioning. Considering the power consumption, size, weight, and cost, an atomic clock used in GNSS satellites is not suitable for LEO satellites (Meng et al., 2020). At the same time, the LEO's Doppler measurements are much larger than those in GNSS, which makes the receiver difficult to capture the carrier phase signal. Besides, some LEO constellations do not broadcast the downlink signals that support pseudorange measurements through a calibrated connection between transmission time tags and transmitter clock time (Psiaki, 2021). In this case, LEO satellites Doppler shift opportunistically for navigation is more attractive.

Doppler positioning technique can provide location service when the receiver fails to get range information. Hill (2001) first introduced the principle of GPS instantaneous Doppler positioning. Chen et al. (2014) and Fernández-Hernández and Borre (2016) proposed a combination of Doppler positioning and coarse time to solve the problem that the user cannot provide a priori location. In the LEO constellation, the TRANSIT Navigation System employed less than a dozen of LEO satellites to provide positioning and navigation service with Doppler measurements (Forssell, 1991). Combining GNSS (Jiang et al., 2022), cellular signals (Qiu et al., 2013), height aiding (Tan et al., 2020), TDOA (Zhao et al., 2017), and Inertial Navigation System (INS) (Benzerrouk et al., 2019; Morales et al., 2019), LEO OpNav shows a remarkable potential. But due to the limited by the number of visible LEO satellites, a position fix was not instantaneous only with Doppler observations.

With the various LEO constellations to be built for broadband Internet over the next decade, it will be likely to offer real-time PNT service with the Doppler measurements of LEO satellites. The Geometric Dilution of Precision (GDOP), as a metric related to both the coverage and the positioning of a system, has been widely used to analyze the positioning potential of a large LEO constellation. Morales-Ferre et al (2020) compared code-GDOP with Doppler-GDOP in Amazon Kuiper and SpaceX StarLink constellations. The values of Doppler-GDOP are remarkably bigger than the ones of the code-GDOP, which means the accuracy of Doppler positioning is more sensitive to observation error. McLemore and Psiaki (2021) analyzed the GDOP for a LEO constellation leveraging Doppler shift and pseudorange measurements simultaneously under a new Doppler positioning model estimating the position vector components, receiver clock offset, velocity vector components, and receiver clock offset rate. Tan et al. (2019) analyzed the effects of measurement errors, satellite orbit errors, and constellation geometric distributions on LEO Doppler positioning performance. To track the Doppler measurements of the multi-constellation LEO satellite's downlink signals for OpNAV, an accurate receiver was designed, and the positioning error is about 132 m with one Orbcomm and two Iridium satellites (Farhangian & Landry, 2020). Benefitting from the spatial and spectral diversity of LEO constellations, an error of less than 23 m is obtained with four Iridium and one Orbcomm satellites ignoring the receiver's velocity (Orabi et al., 2021). In addition, the Doppler shift measurements of GNSS give the opportunity to obtain reliable and high-precision velocity, while the receiver fails to receive effective GNSS satellite signals and is unfavorable for velocity determination in an obscured area. Shtark and Gurfil (2021) determined the receiver's position by TDOA and velocity by Doppler in an LEO constellation and achieved the accuracy of velocity determination at centimeter-level using the extend Kalman filter with dynamical model suitable for the reference model.

In all, the most studies on the LEO PNT service have focused on LEO enhanced GNSS PPP and RTK with large LEO constellations, but less on LEO Doppler positioning. Although there are some initial results in LEO Doppler positioning with measured data, the accuracies of instantaneous positioning and velocity are limited by the number of visible LEO satellites. Meanwhile, few experiments were conducted for the comprehensive investigation of instantaneous velocity determination and positioning with the Doppler shift measurements of a large LEO constellation.

Velocity determination and positioning are two important aspects of GNSS/LEO PVT service. Considering the different applications, we first investigate the performance of velocity determination by using LEO Doppler observations, and then extend to the positioning model and performance analysis. The structure of this paper is arranged as follows. In "Methods" section introduces the detailed simulations of LEO Doppler observations as well as the models of LEO instantaneous velocity determination and positioning. In "Processing strategy" section describes the experimental setup. The results and corresponding analysis are given in "Results and analysis" section. Finally, the main conclusions are drawn in "Conclusions" section.

Methods

In this section, we develop an approach of simulating Doppler shift observations for ground stations and the velocity measurement models for different constellations. Meanwhile, we introduce the measurement model of LEO Doppler positioning considering position, velocity, and clock offset rate of a receiver with seven or more visible LEO satellites.

Doppler simulation

Doppler shift measurements of a receiver are extracted by differencing the received signal frequency and nominal carrier frequency. In this study, we simulate the Doppler shift measurements of GPS and LEO constellations for ground stations. Note that the same wavelength and signal frequency of GPS, L1 and L2 bands, are adopted in LEO satellites.

The Doppler shift measurement can be expressed by (Kassas et al., 2021)

$$D_{r,j}^{s} = -\frac{f_j}{c}\overline{\rho}_{r,j}^{s} \tag{1}$$

where subscript s, r, and j denote the satellite, receiver and carrier frequency, respectively; c is the speed of light and f is the nominal carrier frequency; and $\overline{\rho}_{r,j}^{s}$ means the range rate from receiver to satellite.

The range rate measurement is given by

$$\begin{aligned} -\lambda_j \cdot D_{r,j}^{s} = \bar{\rho}_{r,j}^{s} = \left[\overline{\boldsymbol{r}}_r - \overline{\boldsymbol{r}}^{s}\right]^{T} \cdot \frac{[\boldsymbol{r}_r - \boldsymbol{r}^{s}]}{\|\boldsymbol{r}_r - \boldsymbol{r}^{s}\|_2} \\ + c\left(\delta\bar{t}_r - \delta\bar{t}^{s}\right) - \delta\bar{I}_{r,j}^{s} + \delta\overline{T}_{r,j}^{s} + \delta\overline{R}_{r}^{s} + \varepsilon_{r,j}^{s} \end{aligned} \tag{2}$$

where λ is the carrier wavelength; $\boldsymbol{r}^{s} = [x^{s}, y^{s}, z^{s}]^{\mathrm{T}}$ and $\boldsymbol{r}_r = [x_r, y_r, z_r]^{\mathrm{T}}$ represent the coordinates of satellite and receiver, respectively; $\overline{\boldsymbol{r}}^{s} = [v_x^{s}, v_y^{s}, v_z^{s}]^{\mathrm{T}}$ and $\overline{\boldsymbol{r}}_{\boldsymbol{r}} = [v_{r,x}, v_{r,y}, v_{r,v}]^{\mathrm{T}}$ are the receiver and satellite's three-dimensional velocity vectors, respectively; $\delta\bar{t}_r$ and $\delta\bar{t}^{s}$ are the clock drifts of receiver and satellite, respectively; $\delta\bar{I}_{r,j}^{s}$ and $\delta\overline{T}_{r}^{s}$ are the drifts of the ionospheric and tropospheric delays, respectively; $\varepsilon_{r,j}^{s}$ denotes all non-modeled error sources including the observational noise and multipath error; and $\delta\overline{R}_{r}^{s}$ denotes the Sagnac effect delay rate which can be derived from:

$$\delta\overline{R}_{r}^{s} = \frac{\omega_e}{c}\left[v_y^{s}x_r + y^{s}v_{r,x} - v_x^{s}y_r - v_{r,y}x^{s}\right] \tag{3}$$

where ω_e denotes the earth rotation angular velocity.

The LEO Doppler shift observations are simulated for nine MGEX stations located in different latitudes, are shown in Table 1. Besides, the Doppler shift observations in dynamic scene are also simulated. The varying accelerated motion, uniform motion and constant-acceleration motion are included in dynamic scene. Figure 1 shows the simulated horizontal velocity and acceleration of vehicle in dynamic scene. The LEO constellation consists of 288 satellites, operating in an orbit altitude of 1000 km with a 90° inclination angle, and uses a Walker 288/12/6 constellation geometry. This scheme was adopted in the American Teledesic constellation (Matossian, 1998), and shows a great potential in positioning according to the study of LEO enhanced GNSS PPP and RTK. More importantly, this configuration provides at least 7 visible LEO satellites at any time, which makes instantaneous Doppler positioning possible all over the world. To analyze the performance of LEO and its augmentation for GNSS, GPS Doppler observations are used as well for comparison. Although the real measurements can currently be collected from 31 available GPS satellites in orbit, 24 GPS satellites using the nominal constellation configuration (DOD, 2008) are simulated for the fair comparison of LEO with GPS in the same simulation conditions.

Table 1 Distribution of the selected MGEX stations

Station	Nation	Latitude/(°)	Longitude/(°)
ABMF	France	16.262	−61.528
NRMG	France	−22.228	166.485
MCHL	Australia	−26.359	148.145
LPGS	Argentina	−34.907	−57.932
ULAB	Mongolia	47.865	107.052
BAIE	Canada	49.187	−68.263
ONSA	Sweden	57.396	11.925
SCOR	Denmark	70.485	−21.950
NYA2	Norway	78.930	11.859

In the Doppler observation simulation, the major work is to calculate all the components on the right side of Eq. (2). The station coordinates are fixed to the values given by International GNSS Service (IGS), and the position of the satellite is produced by Systems Tool Kit (STK) software (available online: https://www.agi.com/products/stk). For a moving vehicle, the position and velocity are calculated according to different motion modes. The clock drifts of station and vehicle are simulated as white noise. The velocity and clock drift of a satellite are computed as the average change rate of position and clock offset, respectively. The GFZ multi-GNSS precise clock product is employed to offer the GNSS satellites' clock

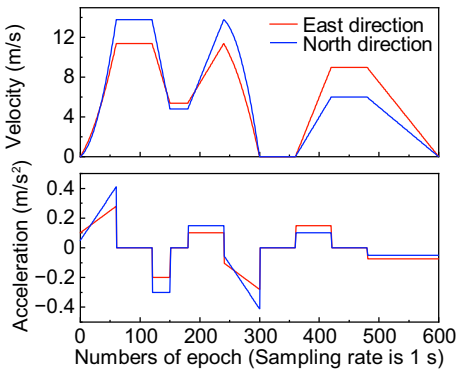

Fig. 1 Simulated horizontal velocity and acceleration of a vehicle in dynamic scene

offsets, while the LEO satellites' clock offsets adopt the records of GPS satellites. The ionospheric delay rate can achieve approximately 18 m/s in Obrcomm LEO satellites (Kassas et al., 2021). In this study, the changes in the ionospheric delay rates are not considered since the method similar to the Ionospheric-Free (IF) combination in the PPP model is used in Doppler positioning and velocity determination. For LEO Doppler observations, Khalife and Kassas (2019) demonstrated that the changes in tropospheric delay rates were negligible. Normally, the atmosphere changes slowly, and the sampling interval of observations is at second level. Therefore, the influence of the changes in tropospheric delay rates is usually not considered for GPS (Wang et al., 2007). In general, the influence of the troposphere is not simulated. In order to ensure the simulated Doppler shift observations close to real data, the random noise obeys the zero-mean normal distribution with a Standard Deviation (STD) dependent on the satellite elevation angle. The STD of each frequency is set to 0.01 m/s for GPS Doppler shift observation in the zenith direction. However, it is worth mentioning that whether the above setting is achievable for LEO constellation depends on the received signal's carrier-to-noise ratio, form of the frequency discriminator, and many other factors (Psiaki, 2021). The different noise levels are set to 0.01 m/s, 0.03 m/s and 0.1 m/s for LEO Doppler observations in the same way. It is noticed that the default noise in LEO is 0.01 m/s equal to GPS Doppler noise.

Velocity estimation

In the velocity determination, the approximate positions of a receiver are known and the linear equations of velocity determination model from Eq. (2) using Doppler observations in GPS and LEO constellations can be written as:

$$\begin{aligned} -\lambda_{j,s}\cdot D^s_{r,j} =& \overline{\rho}_0 + \boldsymbol{u}^s_r\cdot\left[\overline{\boldsymbol{r}}_r - \overline{\boldsymbol{r}}^s\right] \\ &+ c\left(\delta\overline{t}_r - \delta\overline{t}^s\right) - \delta\overline{I}^s_{r,j} \\ &+ \delta\overline{T}^s_r + \delta\overline{R}^s_r + \varepsilon^s_{r,j} \end{aligned} \tag{4}$$

where $\overline{\rho}_0$ is the initial range rate and $\boldsymbol{u}$ is the unit vector of the direction from a receiver to a satellite. In velocity determination, a method similar to IF linear combination in PPP is used to eliminate the first-order ionospheric delay rate. In the model of velocity determination, the IF combination equation can be written as

$$\begin{aligned} -\lambda_{IF,s}\cdot D^s_{r,IF} =& \overline{\rho}_0 + \boldsymbol{u}^s_r\cdot\left[\overline{\boldsymbol{r}}_r - \overline{\boldsymbol{r}}^s\right] \\ &+ c\left(\delta\overline{t}_r - \delta\overline{t}^s\right) + \delta\overline{T}^s_r \\ &+ \delta\overline{R}^s_r + \varepsilon^s_{r,IF} \end{aligned} \tag{5}$$

where $\lambda_{IF,S}$ is the wavelength of IF carrier phase of a satellite. $\varepsilon^s_{r,IF}$ are the sum of measurement noises and un-modeled errors of IF Doppler observations. The unknown parameters vector is:

$$\boldsymbol{X} = \left[\,\overline{\boldsymbol{r}}^{\mathrm{T}}_r \;\; c\delta\overline{t}_r\,\right] \tag{6}$$

where the velocity and clock drift of the receiver are to be estimated.

Doppler positioning

If satellite Doppler-shift measurement is recorded by a receiver on the earth surface, without considering any errors, all points with the same measurement form a circular conical surface (Tan et al., 2019), as shown in Fig. 2. The position of the receiver can be determined by the intersection of these conical surfaces, while the position is the intersection of spherical surfaces in GNSS pseudorange and carrier phase measurement. Limited by the number of available LEO satellites, the Doppler positioning can be achieved using multi-epoch observations, and the movement state of the receiver changes slowly. Beneficial from the spatial and spectral diversity of the LEO constellations, the receiver position can be calculated by the Doppler measurements instantaneously when enough LEO satellites can be observed simultaneously. Equation (2) can be linearized to obtain the coefficient matrix. The linearization can be completed with the first-order Taylor expansion of the equation at a certain point, which can be expressed as:

$$\begin{aligned} -\lambda_{j,L}\cdot D^L_{r,j} =& \overline{\rho}_0 + \boldsymbol{e}^L_r\cdot\boldsymbol{dr} + \boldsymbol{u}^L_r\cdot\boldsymbol{d\overline{r}} + c\left(\delta\overline{t}_r - \delta\overline{t}_{r,0}\right) \\ &- c\delta\overline{t}^s - \delta\overline{I}^L_{r,j} + \delta\overline{T}^L_r + \delta\overline{R}^L_r + \varepsilon^L_{r,j} \end{aligned} \tag{7}$$

with

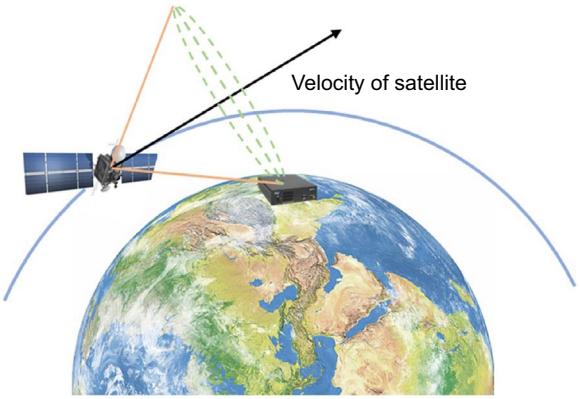

Fig. 2 Doppler effect in satellite positioning

$$\boldsymbol{e}_r^L = \begin{bmatrix} \frac{v_{r,x,0}-v_x^s}{\rho_0} - \frac{(x_{r,0}-x^s)(\bar{r}_{r,0}-\bar{r}^s)\cdot(\boldsymbol{r}_{r,0}-\boldsymbol{r}^s)^T}{\rho_0^3} \\ \frac{v_{r,y,0}-v_y^s}{\rho_0} - \frac{(y_{r,0}-y^s)(\bar{r}_{r,0}-\bar{r}^s)\cdot(\boldsymbol{r}_{r,0}-\boldsymbol{r}^s)^T}{\rho_0^3} \\ \frac{v_{r,z,0}-v_z^s}{\rho_0} - \frac{(z_{r,0}-z^s)(\bar{r}_{r,0}-\bar{r}^s)\cdot(\boldsymbol{r}_{r,0}-\boldsymbol{r}^s)^T}{\rho_0^3} \end{bmatrix}^T$$

where $\overline{\rho}_0$ is the rate of distance change between satellite and receiver, and $\boldsymbol{r}_{r,0} = [x_{r,0}, y_{r,0}, z_{r,0}]^{\mathrm{T}}$, $\bar{\boldsymbol{r}}_{r,0} = \left[v_{r,x,0}, v_{r,y,0}, v_{r,z,0}\right]^{\mathrm{T}}$, and $\delta\bar{t}_{r,0}$ are the initial solution of the receiver's position, velocity, and clock drift, respectively. The combination equations to eliminate ionospheric delay rate can be written as

$$\begin{aligned} -\lambda_{IF,L}\cdot D_{r,IF}^L =& \overline{\rho}_0 + \boldsymbol{e}_r^L\cdot\boldsymbol{dr}^T + \boldsymbol{u}_r^L\cdot\boldsymbol{d\bar{r}}^T \\ &+ c\left(\delta\bar{t}_r - \delta\bar{t}_{r,0}\right) - c\delta\bar{t}^s \\ &+ \delta\overline{T}_r^L + \delta\overline{R}_r^L + \varepsilon_{r,IF}^L \end{aligned} \tag{8}$$

An extended Kalman filter is used for solution, and the unknown parameters vector can be expressed as

$$\boldsymbol{X} = \left[\begin{array}{ccc} \bar{r}_r & \bar{r}_r & c\delta\bar{t} \end{array}\right] \tag{9}$$

Although the motion of the receiver may be complex, the so called "Constant Velocity (CV) model" is commonly used to construct the state transition equation for the low dynamic receiver (Yang et al., 2001), that is

$$\begin{bmatrix} r_r \\ \bar{r}_r \end{bmatrix}_{k,k-1} = \boldsymbol{\Phi}_{k,k-1}\begin{bmatrix} r_r \\ \bar{r}_r \end{bmatrix}_{k-1} + \boldsymbol{W}_k \tag{10}$$

where $\boldsymbol{\Phi}_{k,k-1} = \begin{bmatrix} \mathbf{I}_{3\times3} & \Delta t\cdot\boldsymbol{I}_{3\times3} \\ \mathbf{0}_{3\times3} & \mathbf{I}_{3\times3} \end{bmatrix}$ is the state transition matrix, and Δt is time interval; $\left[\begin{array}{cc} \mathbf{r}_r & \bar{\mathbf{r}}_r \end{array}\right]_{k,k-1}^T$ is the predicted value of the receiver state at epoch k and $\mathbf{W}_k$ is the process noise. Considering that the CV model cannot fully reflect the real motion of the receiver, the process noise should be properly set in different scenes.

Processing strategy

In this section, the configuration of simulation and processing strategies of data are introduced in detail. The different processing strategies are used to evaluate the performance of LEO instantaneous velocity determination and positioning.

In the processing, the precise ephemeris is used to calculate the position, velocity and clock drift of a satellite. The orbit and clock bias errors are simulated in the precise ephemeris. The combination of a cosine function trend term + constant trend term + Gaussian noise (Ma, 2021) is simulated for the ephemeris errors. Figure 3 shows the RMSEs of all satellite orbit errors and clock offset errors in GPS and LEO constellations, respectively.

Table 2 summarizes the data processing strategy for velocity determination and positioning. In the velocity determination, the coordinates of a receiver with different levels of approximation are used to linearize the observation equation. For comparisons, the performances of GPS and GPS + LEO are presented as well to assess the accuracy of velocity determination with LEO enhancing GPS. To correct the ionospheric delay rate effect, a method similar to the IF combination in PPP is adopted in velocity determination. The troposphere delay rate is not considered. As for Sagnac effect delay rate, Eq. (3) is used to correct. The weight of the satellite's Doppler shift observation depends on the satellite elevation.

The performance of the LEO Doppler positioning in the static, static simulated kinematic, and dynamic tests are evaluated. For the static test, the initial velocity is set to 0, and the processing noise of position and velocity are respectively set as $\mathrm{D}\left(W_{r,k}\right) = \begin{bmatrix} 0 & & \\ & 0 & \\ & & 0 \end{bmatrix}$ and $\mathrm{D}(\boldsymbol{W}_{\bar{\mathbf{r}},k}) = \begin{bmatrix} (0.01\,\mathrm{cm/s})^2 & & \\ & (0.01\,\mathrm{cm/s})^2 & \\ & & (0.01\,\mathrm{cm/s})^2 \end{bmatrix}$. For the kinematic test, two schemes with different levels of processing noise are taken for a comparative analysis. Considering that the maximum acceleration of motor vehicles is usually less than 3.0 m/s^2 (Bokare & Maurya, 2017) and the sampling interval is 1 s, the variance of velocity processing noise is set as $\mathrm{D}(\boldsymbol{W}_{\bar{\mathbf{r}},k}) = \begin{bmatrix} (3.0\mathrm{m/s})^2 & & \\ & (3.0\mathrm{m/s})^2 & \\ & & (3.0\mathrm{m/s})^2 \end{bmatrix}$ and the corresponding variance of position processing noise is set as $\mathrm{D}(\boldsymbol{W}_{\mathbf{r},k}) = \begin{bmatrix} (1.5\mathrm{m})^2 & & \\ & (1.5\mathrm{m})^2 & \\ & & (1.5\mathrm{m})^2 \end{bmatrix}$ in scheme 1. In scheme 2, if the carrier is known to be in uniform motion, the variance of position processing noise is set as $\mathrm{D}(W_{r,k}) = \begin{bmatrix} 0 & & \\ & 0 & \\ & & 0 \end{bmatrix}$, and the variance of velocity processing noise is set as $\mathrm{D}(\boldsymbol{W}_{\bar{\mathbf{r}},k}) = \begin{bmatrix} (0.1\mathrm{m/s})^2 & & \\ & (0.1\mathrm{m/s})^2 & \\ & & (0.1\mathrm{m/s})^2 \end{bmatrix}$. For the dynamic test, the processing noise levels of position and velocity are the same as those of scheme 1 in the kinematic test. The clock drift of the receiver is estimated at each epoch as white noise. Besides the same strategies for the drifts of ionosphere and troposphere delays are used in Doppler positioning.

There is a difference between LEO and GNSS positioning because the geocentric position is not available as the initial value of the iteration in the data

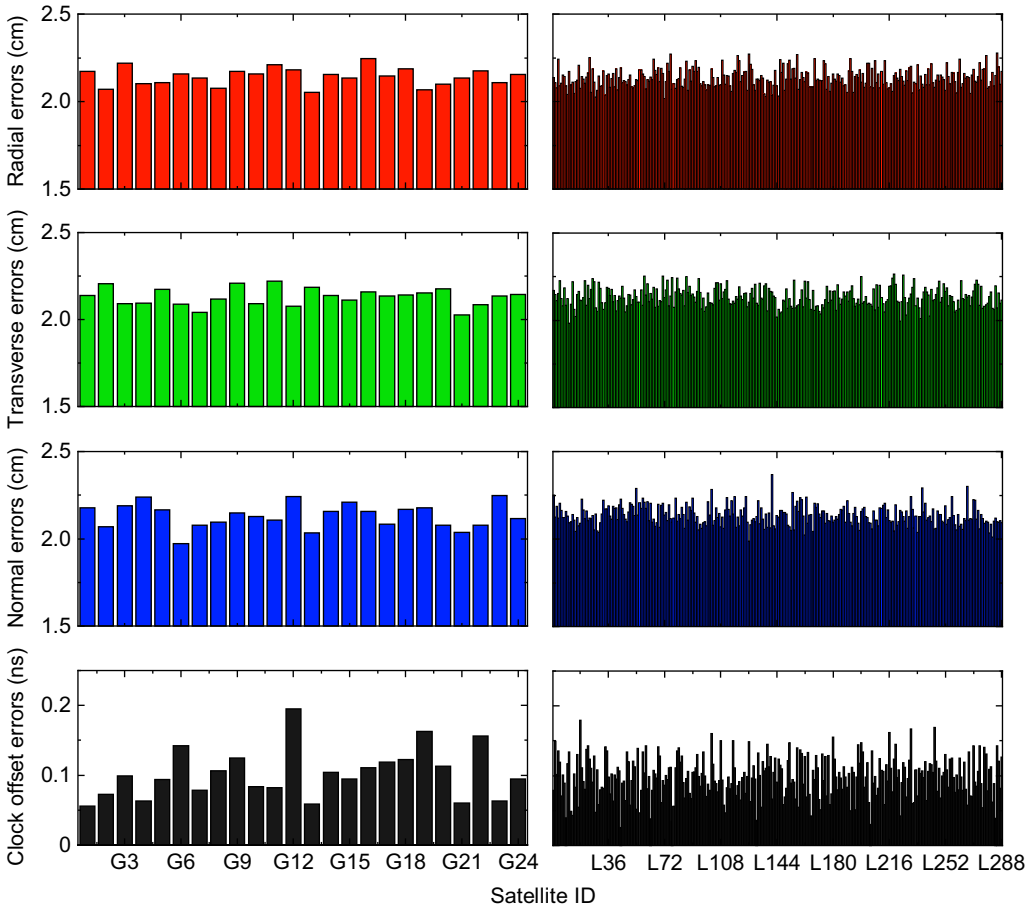

Fig. 3 RMS of GPS and LEO satellites orbit errors in the radial, transverse, normal directions, and clock offset errors

processing. The reason is that the GNSS satellite is much farther from the ground than the earth surface from its center, and the linearization error of the observation equation has little effect under the geocentric position as an initial value. However, the linearization results have a great error due to the much smaller value of LEO orbital altitude than earth radius, leading to the non-convergence of iteration with the geocentric position as an initial value, and thus it is necessary to give the approximate coordinates in LEO Doppler positioning. In this study, the position estimate was initialized 1 km away from the true position in all directions.

Results and analysis

With the simulated Doppler shift observations of GPS and LEO, nine MGEX stations are chosen to evaluate the performance of instantaneous LEO velocity determination and positioning in different latitudes. The performance of LEO and LEO enhanced GPS in velocity determination is analyzed respectively. Doppler positioning experiments are also conducted to test its effectiveness in the static, static simulated kinematic, and dynamic scenes. Besides, the different noise levels of observations are introduced respectively in the static LEO Doppler positioning.

Performance of LEO velocity determination

Figure 4 shows the error of velocity determination with different initial coordinates and visible LEO Satellite Vehicle (SV) at station SCOR. As shown in Fig. 4, the errors in east and north directions are within 3 cm/s, and it is mostly within 6 cm/s in the up direction with the initial coordinate errors of 0.1 m and 1 m. However, there are systematic deviations in three directions with 10 m initial coordinate error. A position bias of 10 m causes horizontal and vertical errors within 6 cm/s and 10 cm/s, respectively. The error of the receiver position will decrease the accuracy of velocity determination because it introduces the computational errors in the design matrix. According to Eq. (4), the impact of the initial receiver position error on the ranging rate can be

Table 2 Data processing strategy

Items	Velocity determination	Positioning
Satellites	LEO, GPS and GPS + LEO	LEO
Estimator	Least square method	Extend Kalman filter
Signal	GPS: L1/L2; LEO: L1/L2	LEO: L1/L2
Sampling rate	1 s	
Elevation cutoff	7°	
Weight scheme	Elevation-dependent weight	
Drift of ionospheric delay	IF combination	
Drift of tropospheric delay	–	
Sagnac effect delay rate	Equation (3)	
Satellite position and velocity	Simulated precise satellite orbit file	
Clock drift of satellite	Simulated precise clock file	
Receiver coordinate	Approximate coordinates	Static: estimated; kinematic: estimated with process noise (scheme1: (1.5, 1.5, 1.5 m)^2; scheme2: 0, 0, 0); dynamic: estimated with process noise ((1.5, 1.5, 1.5 m)^2)
Clock drift of receiver	Estimated	Estimated, white noise
Receiver velocity	Estimated	Static: estimated with process noise (0.01, 0.01, 0.01 cm/s)^2; kinematic: estimated with process noise (scheme1: (3.0, 3.0, 3.0 m/s)^2; scheme2: (0.1, 0.1, 0.1 m/s)^2); dynamic: estimated with process noise ((3.0, 3.0, 3.0 m/s)^2)

expressed as $-\lambda_j \cdot D^s_{r,j} = [\bar{r}_r - \bar{r}^s]^T \cdot \frac{\mathrm{d}\boldsymbol{r}}{\|\boldsymbol{r}_r - \boldsymbol{r}^s\|_2}$. If the magnitude of the receiver position error is 10 m, its impact on the ranging rate will be 7.35 cm/s when $\|r_r - r^s\|_2$ and $\bar{r}^s$ are approximately 1000 km and 7.35 km/s, respectively, which is different from GPS. In GPS, the impact of 10 m position bias on the ranging rate will be 1.6 mm/s (Wang et al., 2007).

Figure 5 shows the RMSE of LEO velocity determination with respect to different initial coordinates of Station SCOR. There is a linear relationship between the velocity accuracy in three directions and the initial coordinate error. As the initial coordinate error increases from 0.1 to 10 m, the RMSEs in east, north, and up components increase from 0.73 cm/s, 0.68 cm/s, and 1.67 cm/s to 2.65 cm/s, 2.96 cm/s, and 4.15 cm/s, respectively. Figure 6 shows the RMSEs of LEO velocity determination and the average number of visible LEO satellites at nine MGEX stations. The performance of velocity determination is

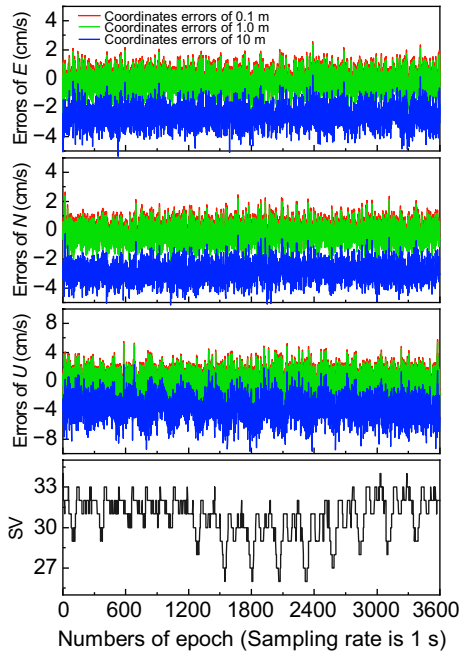

Fig. 4 Errors of velocity determination in the east (E), north (N), and up (U) directions with different initial coordinates and visible LEO satellites vehicle (SV) at station SCOR

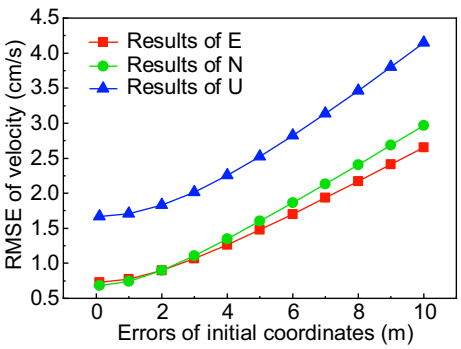

Fig. 5 RMSE of LEO velocity determination in the east, north, and up directions with different initial errors of coordinates at station SCOR

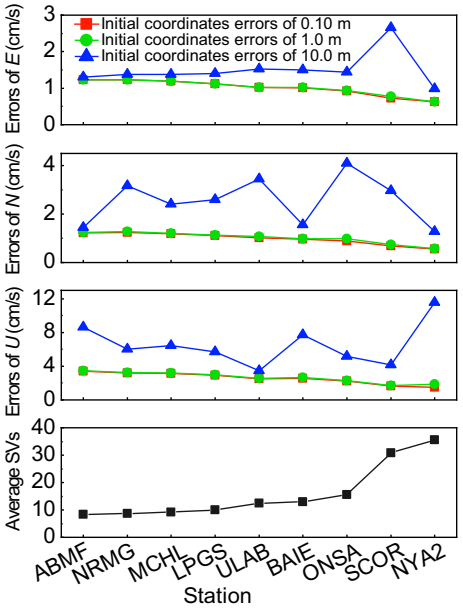

Fig. 6 RMSEs of LEO velocity determination in the east (E), north (N), and up (U) directions with 0.1 m, 1 m, 10 m initial position errors and the average number of available LEO satellites at nine MGEX stations

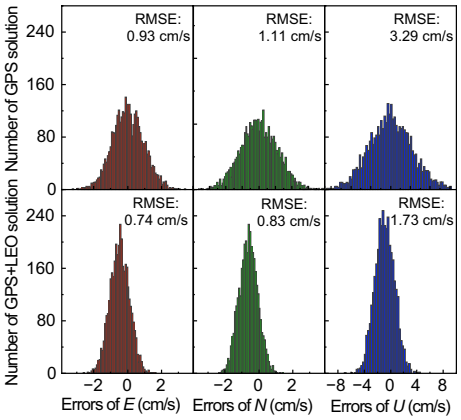

Fig. 7 Error distribution of GPS and GPS + LEO velocity determination, and corresponding RMSEs in the east (E), north (N), and up (U) directions at station SCOR

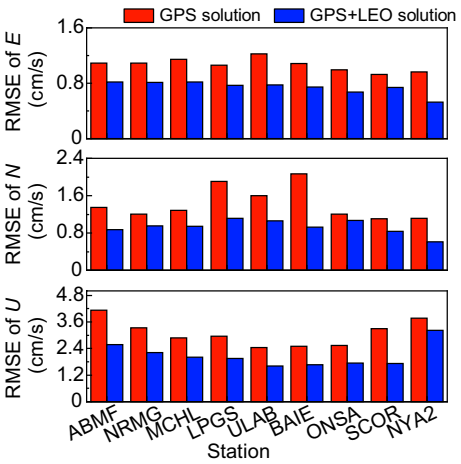

Fig. 8 RMSEs of GPS, LEO and GPS + LEO velocity determination in the east (E), north (N), and up (U) directions at nine MGEX stations

closely related to the latitude of station and number of available satellites with the 0.1 m and 1 m initial position errors. With the increase of latitude, the number of visible LEO satellites increases due to the feature of the polar-orbiting constellation, and thus the corresponding RMSE decreases. For station ABMF, the RMSEs are, respectively, 1.23 cm/s, 1.23 cm/s, and 3.39 cm/s in the east, north, and up directions with an average number of 8.4 LEO satellites and 0.1 m initial position error. As for the high-latitude station NYA2, the average number of visible LEO satellites reaches 35.5, and the corresponding RMSEs of velocity determination are reduced to 0.62 cm/s, 0.56 cm/s, and 1.48 cm/s in the east, north, and up directions, respectively.

For a comparison, the results of velocity determination with different constellation schemes, i.e. GPS and GPS + LEO, are analyzed. Figure 7 shows the error distribution of velocity determination in the east, north, and up directions at station SCOR with 3.0 m initial coordinate error (considering the absolute GPS positioning precision). For the GPS scheme, the RMSEs are, respectively, 0.93 cm/s, 1.11 cm/s, and 3.29 cm/s in the east, north, and up components, which are comparable to the accuracy of LEO according to Fig. 5. For the GPS + LEO scheme, the accuracy is significantly improved in all directions, and the RMSEs are 0.74 cm/s, 0.83 cm/s, and 1.73 cm/s, respectively. Figure 8 shows the RMSEs of velocity determination at nine MGEX stations with two different schemes. The RMSE values are within 1.11 cm/s in horizontal and 3.21 cm/s in vertical for all stations with GPS and LEO satellites. To conclude, the LEO Doppler shift observations contribute to GPS velocity determination.

Performance of LEO Doppler positioning

In order to evaluate the performance of Doppler in positioning, the results of static, static simulated kinematic and dynamic tests are presented. Three stations, MCHL, ONSA and NYA2, located at different latitudes are selected as examples to analyze the LEO positioning performance. The performance of positioning in dynamic scene is evaluated in high latitude region.

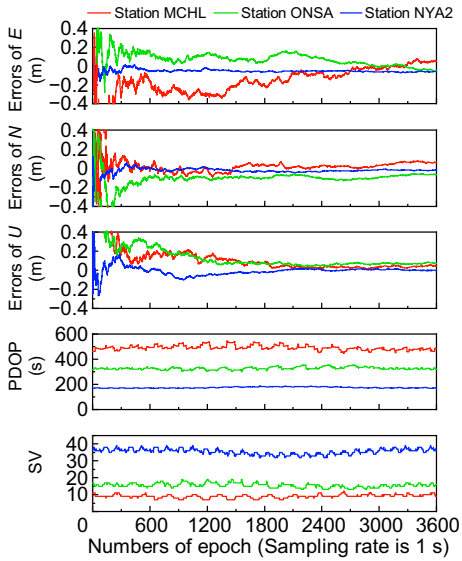

Fig. 9 Static Doppler positioning solutions in east (E), north (N), and up (U) directions at station MCHL, ONSA, and NYA2. The corresponding PDOP values and numbers of LEO satellites vehicle (SV) are also shown

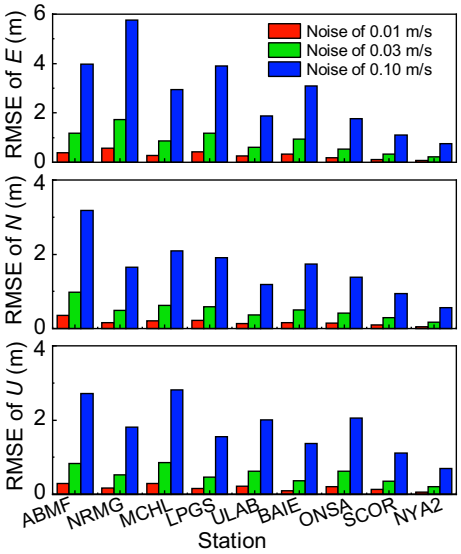

Fig. 10 RMSEs of static Doppler positioning with different noise levels at nine stations

Static Doppler positioning

Figure 9 shows static Doppler positioning results at MCHL, ONSA, and NYA2. It can be found that high accuracy can be achieved with different convergence time at three stations. The positioning results are more stable in three directions at high latitude station because of more visible LEO satellites. Besides, the solution convergence of Doppler positioning is significantly improved at high latitude station. It is worth noting that the position errors are less than 0.1 m in three directions after about 6 min at NYA2 with 35.5 average visible LEO satellites. Figure 9 also shows the corresponding total numbers of visible satellites and PDOP values. The detailed method of calculating PDOP in Doppler positioning is introduced in the appendix. At the station MCHL, the average number of visible satellites is 9.1 and the PDOP value is 491.4. The corresponding visible satellite number is increased by 26.4, and the average PDOP values is decreased to 174.9 at the station NYA2. Assuming that the noise of LEO Doppler measurements is 0.01 m/s, the position accuracy can achieve about 1.75–4.91 m, which is comparable to the positioning accuracy of GNSS pseudorange positioning.

To analyze the potential of static Doppler positioning, the RMSEs of the east, north, and up components during the test period are summarized in Table 3. For the nine stations, the RMSEs can achieve sub-meter level at three directions. It is worth noting that the RMSEs can achieve centimeter at high-latitude station NYA2.

In order to analyze the accuracy of static LEO Doppler positioning with different noise levels, Fig. 10 shows the results of static LEO Doppler positioning with different noise levels configuration at nine stations. We can find that the accuracy of static positioning can reach decimeter-level with noise levels of 0.01 m/s and 0.03 m/s, but meter-level with noise of 0.10 m/s. Meanwhile, at higher latitude stations the accuracy can be improved due to more satellites.

Static simulated kinematic Doppler positioning

Figure 11 shows the results of kinematic Doppler positioning for scheme 1. The accuracy of position can reach meter level. More LEO satellites can improve the accuracy of kinematic Doppler positioning. The RMSEs of

Table 3 RMSE of positioning errors at nine MGEX stations in static Doppler positioning

Station	ABMF	NRMG	MCHL	LPGS	ULAB	BAIE	ONSA	SCOR	NYA2
E (m)	0.39	0.57	0.28	0.42	0.25	0.34	0.19	0.11	0.08
N (m)	0.35	0.15	0.21	0.21	0.14	0.16	0.14	0.10	0.05
U (m)	0.29	0.17	0.29	0.16	0.22	0.10	0.21	0.14	0.06

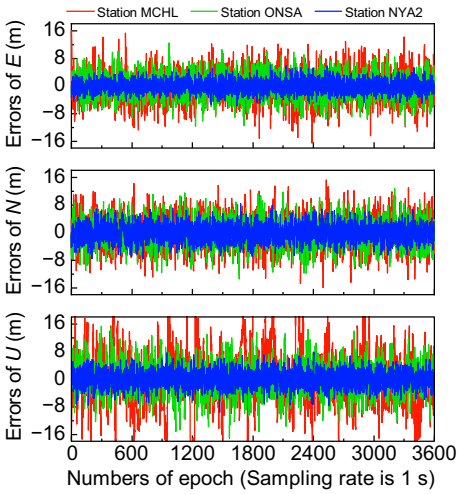

Fig. 11 Results of kinematic Doppler positioning solutions in the east (E), north (N) and up (U) directions, respectively, at station MCHL, ONSA and NYA2 for scheme 1

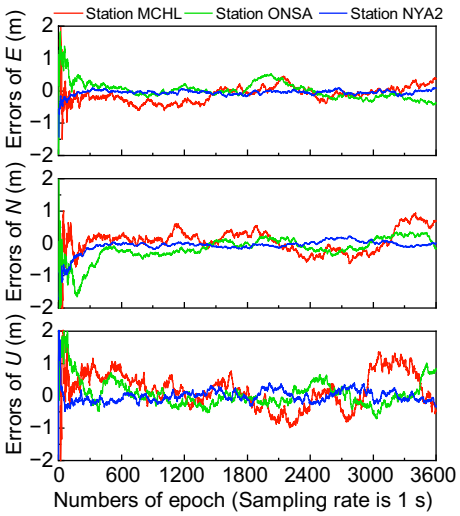

Fig. 12 Results of kinematic Doppler positioning solutions in the east (E), north (N) and up (U) directions, respectively, at station MCHL, ONSA and NYA2 for scheme 2

position at different stations are given in Table 4. The average RMSEs are 3.66 m, 3.97 m, and 5.93 m in the east, north, and up directions, respectively.

Figure 12 shows the kinematic solutions of LEO Doppler positioning for scheme 2. Compared with Fig. 10, the position results are more stable and the accuracy in three directions are improved. Table 5 shows the corresponding positioning errors at nine stations. For the low- and mid-latitude stations, the RMSEs are approximately 0.3–0.6 m in the horizontal and 0.5–1.0 m in the vertical. For the high-latitude stations, the RMSEs of position reduce to 0.1–0.3 m in the horizontal and 0.2–0.4 m in the vertical. The averages RMSEs are 0.38 m, 0.41 m, and 0.67 m in three directions, respectively.

Dynamic Doppler positioning

As mentioned before, a dynamic scene in high latitude region is simulated, and the motion state is shown in Fig. 1. Figure 13 shows the results of Dynamic Doppler positioning. The errors in three directions are all within 10.0 m, and the positioning accuracies are almost the same for different motion modes. The average RMSEs are respectively, 2.24 m, 3.15 m, and 3.23 m in the east, north and up directions. The accuracy is consistent with the result of scheme 1 in simulated kinematic Doppler positioning at high latitude stations.

Conclusions

This paper investigates the performance of instantaneous LEO velocity determination and positioning using Doppler observations from a LEO constellation.

For LEO Doppler velocity determination, the test indicates that the accuracy is closely related to the initial receiver position error. Statistical results show that with the increase of initial receiver position error from 0.1 to 10 m, the RMSEs of LEO velocity determination increase from 0.73 to 2.65 cm/s, 0.68 to 2.96 cm/s, and 1.67 to 4.15 cm/s in the east, north, and up directions, respectively. There are systematic deviations in three directions with an initial coordinate error of 10 m. Meanwhile, more available LEO satellites can improve the velocity determination accuracy. Compared with GPS, the accuracy of velocity determination with GPS + LEO can be improved, and the RMSEs are within 1.11 cm/s in the horizontal and 3.21 cm/s in the vertical.

Different from GNSS positioning, LEO Doppler positioning has large PDOP, even if more than 30 visible LEO satellites are available, its PDOP values can reach several

Table 4 RMSEs of kinematic Doppler positioning solutions at nine stations for scheme 1

Station	ABMF	NRMG	MCHL	LPGS	ULAB	BAIE	ONSA	SCOR	NYA2
E (m)	4.71	4.73	4.37	4.48	3.84	3.79	3.32	2.21	1.67
N (m)	4.82	4.58	4.48	4.46	3.95	3.92	3.77	3.41	2.33
U (m)	9.31	7.91	8.04	6.89	3.84	5.56	4.42	3.09	2.23

Table 5 RMSEs of kinematic Doppler positioning solutions at nine stations in scheme 2

Station	ABMF	NRMG	MCHL	LPGS	ULAB	BAIE	ONSA	SCOR	NYA2
E (m)	0.48	0.60	0.48	0.50	0.35	0.48	0.27	0.19	0.12
N (m)	0.55	0.51	0.45	0.44	0.47	0.29	0.41	0.29	0.22
U (m)	0.90	1.04	0.83	0.79	0.79	0.48	0.62	0.42	0.20

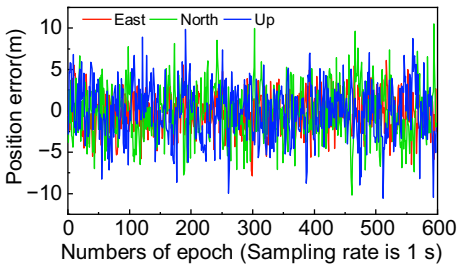

Fig. 13 Errors of dynamic Doppler positioning solution in the east (E), north (N) and up (U) directions

achieved instantaneously (epoch-wise) with the same Doppler measurement error as GPS, i.e., 0.01 m/s, which means it is comparable to the accuracy of GNSS pseudorange positioning. The performance of Doppler positioning is analyzed in static, static simulated kinematic, and dynamic scenes, respectively, and the CV model is used in EKF. In the static scene, the RMSEs of position are few decimeter level, and the accuracy can be improved with more satellites available. The RMSEs are 0.05–0.14 m at high-latitude stations. Besides, the effect of measurement noise on Doppler positioning is also investigated. The RMSEs of static positioning can be at decimeter-level with errors of 0.01 m/s and 0.03 m/s, while at meter-level with error of 0.1 m/s. In the kinematic scene, different process levels of noise are set. When the variance of position process noise is $(1.5\ \mathrm{m})^2$ and the variance of velocity process noise is $(3.0\ \mathrm{m/s})^2$, the average RMSEs of position are, respectively, 3.66 m, 3.97 m, and 5.93 m in three directions. In the scheme where the process noise of position is zero and the variance of velocity process noise is $(0.1\ \mathrm{m/s})^2$, the average RMSEs of position are, respectively, 0.38 m, 0.41 m, and 0.67 m. In the dynamic scene, different motion modes are simulated, and the RMSEs are 2.24 m, 3.14 m, and 3.23 m, respectively.

Overall, our initial assessment of LEO Doppler velocity determination and positioning indicates that the LEO Doppler can improve GNSS velocity determination performance and provide a positioning service whose accuracy is comparable to that of GNSS pseudorange positioning. Further studies will evaluate the LEO Doppler positioning performance in harsh environments. The configuration optimization and constellation design of LEO satellites need to be explored. Some limitations in this study include the simulation and processing of atmospheric delay rate may cause distortions, and the approach to reduce the value of PDOP for improving LEO Doppler positioning.

Appendix

When GNSS/LEO broadcasts pseudorange and carrier phase observations, the ionosphere delay, troposphere delay, and ambiguity can be estimated in addition to position and clock error. However, only position and clock error are taken into the calculation of PDOP in the PPP model. In the Doppler positioning model, there are 3D position, 3D velocity, and receiver clock drift to be estimated, but the value of PDOP for Doppler positioning is calculated with the consideration of position and clock drift which can evaluate the basic positioning performance of Doppler positioning. In this case, when calculating the PDOP value of LEO Doppler positioning, the matrix in the observation equation can be expressed as:

$$\mathbf{Z} = \mathbf{H}\left[\, r_r \;\; c\bar{t} \,\right]^T \tag{11}$$

$$\mathbf{H} = \begin{bmatrix} \frac{d\bar{\rho}_{r,j}^{s,1}}{dx_r} & \frac{d\bar{\rho}_{r,j}^{s,1}}{dy_r} & \frac{d\bar{\rho}_{r,j}^{s,1}}{dz_r} & 1 \\ \frac{d\bar{\rho}_{r,j}^{s,2}}{dx_r} & \frac{d\bar{\rho}_{r,j}^{s,2}}{dy_r} & \frac{d\bar{\rho}_{r,j}^{s,3}}{dz_r} & 1 \\ \vdots & \vdots & \vdots & \vdots \\ \frac{d\bar{\rho}_{r,j}^{s,n}}{dx_r} & \frac{d\bar{\rho}_{r,j}^{s,n}}{dx_r} & \frac{d\bar{\rho}_{r,j}^{s,n}}{dx_r} & 1 \end{bmatrix} \tag{12}$$

The challenges must be addressed before calculating the PDOP of Doppler positioning. The value of PDOP describes the influence of measurement error on positioning results, and the units determined by the product of measurement error and PDOP should be meters. The units of $\mathbf{r}_r$ are meters, and the units of $-\lambda_j D_{r,j}^s$ and $c\bar{t}_r$ are m/s. A scaling factor η is introduced to redefine all the parameters having the common units, m/s, which makes the units of matrix H 1/s. The scaling factor can be expressed as

$$\eta = \frac{R_s}{R_s - R_E}\sqrt{\frac{GM}{R_s^3}} \tag{13}$$

where R_s and R_E denote the radius of satellite orbit and earth, respectively, and GM is the gravitational constant of the earth.

This recalling allows the observation equation matrix to be rewritten in the following equivalent form:

$$Z = H_\eta \left[\mathbf{r}_r \;\; c\bar{t}/\eta \right]^T \tag{14}$$

$$H_\eta = \begin{bmatrix} \frac{d\bar{\rho}_{r,j}^{s,1}}{dx_r} & \frac{d\bar{\rho}_{r,j}^{s,1}}{dy_r} & \frac{d\bar{\rho}_{r,j}^{s,1}}{dz_r} & \eta \\ \frac{d\bar{\rho}_{r,j}^{s,2}}{dx_r} & \frac{d\bar{\rho}_{r,j}^{s,2}}{dy_r} & \frac{d\bar{\rho}_{r,j}^{s,2}}{dz_r} & \eta \\ \vdots & \vdots & \vdots & \vdots \\ \frac{d\bar{\rho}_{r,j}^{s,n}}{dx_r} & \frac{d\bar{\rho}_{r,j}^{s,n}}{dy_r} & \frac{d\bar{\rho}_{r,j}^{s,n}}{dz_r} & \eta \end{bmatrix} \tag{15}$$

The next step is to obtain the matrix Q as

$$Q = (H_\eta^T H)^{-1} \tag{16}$$

The PDOP of Doppler positioning can be calculated as

$$PDOP = \sqrt{Q(1,1) + Q(2,2) + Q(3,3)} \tag{17}$$

Acknowledgements
We thank IGS for providing the GNSS observation data and the MGEX products.

Author contributions
Conceptualization and Methodology: FG and YY; Writing original draft: FG and YY; Editing: FG, YY, FM, YZ, and HL; Review: FG, YY, FM, YZ, HL and XZ; All authors read and approved the final manuscript.

Funding
This research was supported by the Fund of National Key Research and Development Program of China (No. 2022YFB3903902), the National Science Fund for Distinguished Young Scholars (No. 41825009), and the Key Research and Development Program of Hubei Province (No. 2022BAA054).

Availability of data and materials
The simulated data are available upon request.

Declarations

Competing interests
The authors declare that they have no competing interests.

Received: 1 August 2022 Accepted: 23 February 2023
Published online: 20 March 2023

References

Benzerrouk, H., Quang, N., Fang, X., Amrhar, A., Nebylov, A V., & Landry R J. (2019). Alternative PNT based on Iridium Next LEO satellites Doppler/INS integrated navigation system. In *2019 26th Saint Petersburg international conference on integrated navigation systems (ICINS)*.

Bokare, P. S., & Maurya, A. K. (2017). Acceleration–deceleration behaviour of various vehicle types. *Transportation Research Procedia, 25*, 4733–4749.

Borio, D., Dovis, F., Kuusniemi, H., & Presti, L. L. (2016). Impact and detection of GNSS jammers on consumer grade satellite navigation receivers. *Proceedings of the IEEE, 104*(6), 1233–1245.

Chen, H., Wang, H., Chiang, Y., & Chang, F. (2014). A new coarse-time GPS positioning algorithm using combined Doppler and code-phase measurements. *GPS Solutions, 18*(4), 541–551. https://doi.org/10.1007/s10291-013-0350-8

DOD SPS, Department of Defense USA. (2008). *Global positioning system standard positioning service performance standard*, 4th edn. http://www.gps.gov/technical/ps/2008-SPS-performancestandard

Enge, P., Ferrell, B., Bennet, J., Whelan, D., Gutt, G., & Lawrence, D. (2012). Orbital diversity for satellite navigation. In *Proceedings of the25th international technical meeting of the Satellite Division of The Institute of Navigation (ION GNSS 2012), Nashville, TN* (pp. 3834–3846).

Farhangian, F., & Landry, R. (2020). Multi-constellation software-defined receiver for Doppler positioning with LEO satellites. *Sensors, 20*(20), 5866.

Fernández-Hernández, I., & Borre, K. (2016). Snapshot positioning without initial information. *GPS Solutions, 20*(4), 605–616. https://doi.org/10.1007/s10291-016-0530-4

Forssell, B. (1991). *Radionavigation systems*. Prentice Hall International.

Ge, H., Li, B., Ge, M., Zang, N., Nie, L., Shen, Y., & Schuh, H. (2018). Initial assessment of precise point positioning with LEO enhanced global navigation satellite systems (LeGNSS). *Remote Sensing, 10*(7), 984. https://doi.org/10.3390/rs10070984

Hill, J. (2001). The principle of a snapshot navigation solution based on Doppler shift. In *Proceedings of the ION GNSS 2001, Institute of Navigation, Salt Lake City, Utah, USA, September 11–14* (pp. 3044–3051).

Ioannides, R. T., Pany, T., & Gibbons, G. (2016). Known vulnerabilities of global navigation satellite systems, status, and potential mitigation techniques. *Proceedings of the IEEE, 104*(6), 1–21.

Jiang, M., Qin, H., Zhao, C., & Sun, G. (2022). LEO Doppler-aided GNSS position estimation. *GPS Solutions, 26*(1), 1–18. https://doi.org/10.1007/s10291-021-01210-2

Kassas, Z. M., et al. (2021). Navigation from low Earth orbit. In Y. J. Morton (Ed.), *Position, navigation, and timing technologies in the 21st century* (pp. 1381–1412). Wiley.

Khalife, J., & Kassas, Z. M. (2019). Assessment of differential carrier phase measurements from orbcomm LEO satellite signals for opportunistic navigation. In *Proceedings of the 32nd International Technical Meeting of the Satellite Division of The Institute of Navigation (ION GNSS+ 2019)* (pp. 4053–4063).

Li, X., Lv, H., Ma, F., Li, X., Liu, J., & Jiang, Z. (2019b). GNSS RTK positioning augmented with large LEO constellation. *Remote Sensing, 11*, 288. https://doi.org/10.3390/rs11030228

Li, X., Ma, F., Li, X., Lv, H., Bian, L., Jiang, Z., & Zhang, X. (2019a). LEO constellation-augmented multi-GNSS for rapid PPP convergence. *Journal of Geodesy, 93*(5), 749–764. https://doi.org/10.1007/s00190-018-1195-2

Lu, J., Guo, X., & Su, C. (2020). Global capabilities of BeiDou navigation satellite system. *Satellite Navigation, 1*, 27. https://doi.org/10.1186/s43020-020-00025-9

Ma, F. (2021). *Research on constellation optimization and signal frequency design for a LEO-based navigation augmentation system*. Ph.D. Thesis, Wuhan University, China

Matossian, M. G. (1998). A teledesic space infrastructure overview. In J. C. van der Ha (Ed.), *Mission design and implementation of satellite constellations. Space technology proceedings.* (Vol. 1). Springer.

McLemore, B., & Psiaki, M. L. (2021). GDOP of Navigation using pseudorange and doppler shift from a LEO constellation. In *Proceedings of the 34th International Technical Meeting of the Satellite Division of The Institute of Navigation (ION GNSS+ 2021)* (pp. 2783–2803).

Meng, Y., Lei, W., Bian, L., Yan, T., & Wang, Y. (2020). Clock tuning technique for a disciplined high medium–long-stability GNSS oscillator with precise clock drifts for LEO users. *GPS Solutions, 24*, 1–15.

Morales, J., Khalife, J., & Kassas, Z. M. (2019). Simultaneous tracking of Orbcomm LEO satellites and inertial navigation system aiding using Doppler measurements. In *IEEE 89th vehicular technology conference (VTC2019-Spring)* (pp. 1–6). IEEE.

Morales-Ferre, R., Lohan, E. S., Falco, G., & Falletti, E. (2020). GDOP-based analysis of suitability of LEO constellations for future satellite-based positioning. In

8th IEEE international conference on wireless for space and extreme environments (WiSEE) (pp. 147–152). IEEE.
Orabi, M., Khalife, J., & Kassas, Z. M. (2021, March). Opportunistic navigation with Doppler measurements from Iridium Next and Orbcomm LEO satellites. In *2021 IEEE Aerospace Conference (50100)* (pp. 1–9). IEEE.
Psiaki, M. L. (2021). Navigation using carrier Doppler shift from a LEO constellation: TRANSIT on steroids. *Navigation, 68*(3), 621–641. https://doi.org/10.1002/navi.438
Qiu, D., De Lorenzo, D. S., & Bhattacharya, T. (2013). Indoor geo-location with cellular RF pattern matching and LEO communication satellite signals. *Proceedings of the 2013 International Technical Meeting of The Institute of Navigation, San Diego, California, 2013* (pp. 726–733).
Shtark, T., & Gurfil, P. (2021). Position and velocity estimation with a low Earth orbit regional navigation satellite constellation. *Proceedings of the Institution of Mechanical Engineers Part G-Journal of Aerospace Engineering, 236*, 1375–1387.
Tan, Z., Qin, H., Cong, L., & Zhao, C. (2019). New method for positioning using Iridium satellite signals of opportunity. *IEEE Access, 7*, 83412–83423. https://doi.org/10.1109/ACCESS.2019.2924470
Tan, Z., Qin, H., Cong, L., & Zhao, C. (2020). Positioning using Iridium satellite signals of opportunity in weak signal environment. *Electronics, 9*(1), 37. https://doi.org/10.3390/electronics9010037
Wang, F., Hu, C., Wu, S., Tao, Y., & Xu, Y. (2020). Research on BeiDou anti-spoofing technology based on comprehensive radio determination satellite service. *Satellite Navigation, 1*(1), 9. https://doi.org/10.1186/s43020-019-0004-2
Wang, F., Zhang, X., & Huang, J. (2007). Error analysis and accuracy assessment of GPS absolute velocity determination with SA off. *Geomatics and Information Science of Wuhan University, 32*(6), 515–519.
Yang, Y., He, H., & Xu, G. (2001). Adaptively robust filtering for kinematic geodetic positioning. *Journal of Geodesy, 75*(2), 109–116.
Zhao, J., Li, L., & Gong, Y. (2017) Joint navigation and synchronization in LEO dual-satellite geolocation systems. In *IEEE 85th vehicular technology conference (VTC Spring)* (pp. 1–5). IEEE.

Publisher's Note